RESEARCH

Thermal entanglement versus quantum-memory-assisted entropic uncertainty relation in a two-qubit Heisenberg system with Herring–Flicker coupling under Dzyaloshinsky–Moriya interaction

Zakaria Bouafia[1] · Mansoura Oumennana[1] · Mostafa Mansour[1] · Fatiha Ouchni[2]

Abstract

In our investigation, we delve into the dynamics of thermal entanglement and quantum-memory-assisted entropic uncertainty relation (QMA-EUR) within an XXZ Heisenberg spin-1/2 chain consisting of two qubits. This system is affected by the Herring–Flicker (HF) coupling and exposed to the Dzyaloshinsky–Moriya (DM) interaction, in the presence of an external homogeneous magnetic field. We assume that the system is in thermal equilibrium with a reservoir and examine how various parameters, including the HF coupling distance R, equilibrium temperature, and other system characteristics, affect the logarithmic negativity used to quantify thermal entanglement and QMA-EUR. Our findings reveal intriguing distinctions in the behaviors of QMA-EUR and thermal entanglement. Notably, an increase in temperature is found to effectively reduce thermal entanglement while simultaneously enhancing QMA-EUR. Furthermore, we notice that bipartite entanglement and QMA-EUR exhibit distinct behaviors as we vary the coupling distance, R. Specifically, the logarithmic negativity attains its highest value at a coupling distance of $R = 1.25$, which coincides with the lowest QMA-EUR value. Furthermore, we discover that the presence of high-intensity magnetic fields has a detrimental influence on the level of thermal entanglement. However through adjustments in the inter-spins relative distance R, the strength of the DM interaction, temperature T, the anisotropy parameter, and the static magnetic field B, it is possible to suppress the QMA-EUR and enhance bipartite entanglement within the system. These findings suggest encouraging possibilities for advancing quantum technologies that make use of this quantum system.

1 Introduction

Quantum entanglement is a strong type of non-classical correlations, making it the key to many applications in quantum computing and information [1]. Consequently, this becomes a pivotal component in advanced quantum information technologies, notably quantum sensing [2], quantum computation [3, 4], quantum cryptography [5, 6], quantum teleportation [7–9], quantum randomness [10], quantum dense coding [11], and so on. Many quantifiers were proposed to quantify the amount of quantum entanglement, such as entanglement of formation, negativity, concurrence, and logarithmic negativity [12–24]. In recent decades, numerous efforts have been undertaken to identify the most effective measure among various alternatives. However, it is difficult to say definitively that one measure is better than the others, as each one offers unique advantages depending on specific conditions. In this context, quantum entanglement has been extensively examined in many papers using different quantifiers [25–30].

The uncertainty principle, initially postulated by Heisenberg [31], lies at the heart of quantum mechanics, crucially illustrating the distinction between the quantum and classical worlds. Since then, Robertson [32] has expanded the concept of the uncertainty principle to encompass any two incompatible observables. Instead of using standard deviation and based on the concept of entropy, other interpretations of the uncertainty principle have been proposed [33–36].

✉ Mostafa Mansour
mostafa.mansour.fsac@gmail.com

[1] Laboratory of High Energy Physics and Condensed Matter Department of Physics, Faculty of Sciences of Aïn Chock, Hassan II University, Casablanca, Morocco

[2] LPMR, Department of Physics, Faculty of Sciences of Oujda, Mohammed Premier University, Oujda, Morocco

In this sense, Berta and his colleagues [37] discovered that the uncertainty principle could be strengthened by taking into consideration an entangled quantum memory associated with the measured particle. Thereby, the concept of quantum-memory-assisted entropic uncertainty relation (QMA-EUR) is highly correlated with the connection of the particle to the quantum memory. Furthermore, it was found that the bound of QMA-EUR can be further refined by taking into account the quantum discord and the classical correlations associated with the measured particle [38]. The QMA-EUR has various potential applications, including probing quantum correlations [38, 39], entanglement witness [40, 41], quantum speed limit [42, 43], quantum cryptography [44], quantum metrology [45], and quantum key distribution [46]. Moreover, the QMA-EUR has been generalized and investigated in various bipartite and multipartite quantum systems [47–54]. In addition, EUR with and without quantum memory were derived for multiple measurements settings [55]. By taking into account the mutual information and the Holevo quantity, Xie et al. further tightened the lower bound of EUR for multiple measurements [56].

Exploring quantum entanglement, non-classical correlations, and QMA-EUR in Heisenberg spin-chain models, is attracting growing interest within the scientific community. Within this domain, numerous researchers have undertaken investigations into quantum resources and QMA-EUR in a variety of bipartite and multipartite quantum systems, including Heisenberg spin-chain models [46, 50, 57–62]. Additionally, there has been extensive scrutiny of the dynamics of quantum resources in a bipartite Heisenberg XXZ model under the influence of Dzyaloshinsky–Moriya (DM) interaction (referenced as [63–65]).

Apart from Heisenberg spin models, EUR and quantumness were investigated in other interesting systems at the intersection between quantum information and elementary particle physics or relativity theory, such as experimentally observed neutron oscillations [66–68] or Dirac fields in the background of Garfinkle–Horowitz–Strominger (GHS)—dilation black holes [69]. However, despite these extensive efforts, a significant gap remains unaddressed in the realm of quantum entanglement and QMA-EUR when considering the XXZ model in conjunction with Herring–Flicker coupling. Hence, it is crucial to spotlight the behaviors of quantum entanglement and QMA-EUR within this framework. In realistic settings, and due to quantum fluctuations, spins are not frozen on their lattice sites, thus it is an interesting prospect to assume that the coupling strength between spins might depend on the distance separating them. Indeed, the Herring–Flicker coupling relies on the inter-spin relative distance (R), offering an insight into its real essence within the Heisenberg XXZ model. Therefore, it is crucial to explore the impact of the distance R on the thermal entanglement and QMA-EUR

in the bipartite Heisenberg XXZ model. Moreover, we aim to study the effects of the DM interaction and an external magnetic field on thermal entanglement while considering the distance R and other system parameters.

Building upon earlier research, specifically investigations into the effects of Herring–Flicker coupling [70, 71], our study delves into the fundamental relationship between bipartite entanglement and QMA-EUR in a two-qubit Heisenberg system with Herring–Flicker coupling. The main objective is to examine how the HF coupling distance affects various quantum indicators within this system in the presence of the Dzyaloshinskii-Moriya (DM) interaction and an external magnetic field. Within this context, Huang and Kais [72] have previously demonstrated the dependence of entanglement in an XY spin chain, governed by the Ising model, on the distance associated with Herring–Flicker coupling [73]. Notably, their research revealed that an increase in the magnetic field strength leads to a reduction in entanglement over the Herring–Flicker coupling distance. This coupling mechanism plays a crucial role in delineating the energy difference between the triplet and singlet states of the hydrogen molecule, as expounded in reference [73]. This difference is quantified as $J(R) = E_{\text{triplet}} - E_{\text{singlet}} = 1.642 \ e^{-2R}R^{5/2} + O(R^2 e^{-2R})$, which implies that the distinction between the symmetric and antisymmetric state energies must be exceedingly small, decaying exponentially as e^{-2R}. Thus, by manipulating the coupling distance, the energy difference becomes adjustable. Building upon these findings, our paper delves into the study of correlations within a bipartite Heisenberg XXZ model. This model includes the Herring–Flicker coupling, the DM interaction, and the external uniform magnetic field. The Herring–Flicker approximation is a valuable tool for gauging the strength of the exchange interaction between the two qubits in the Heisenberg XXZ model. Here, we examine the impact of various factors, including the inter-spin relative distance R, the DM interaction, the anisotropy parameter, the external magnetic field, and the equilibrium temperature, on the variations in thermal entanglement and QMA-EUR within the Heisenberg model under consideration.

We structure our paper, as follows: In Sect. 2, we briefly introduce essential definitions and expressions related to logarithmic negativity ($\mathcal{LN}$) and QMA-EUR. In Sect. 3, we outline the Hamiltonian for the bipartite Heisenberg XXZ model with Herring–Flicker coupling under DM interaction and derive the associated thermal density matrix using Gibbs equation. Section 4 presents and analyzes the behaviors of QMA-EUR and logarithmic negativity within the studied system. In Sect. 5, we summarize the main findings of our research.

2 Quantum indicators

We provide in this section the definitions of QMA-EUR and logarithmic negativity employed in this study to measure, respectively, the measurement uncertainty and the amount of entanglement between the two qubits in the considered system.

2.1 $\mathcal{LN}$

$\mathcal{LN}$ is an extensively used measure of entanglement since it is easy to compute [20, 21]. Given a bipartite density matrix ρ, $\mathcal{LN}$ is given as follows

$$\mathcal{LN}(\rho) = \log_2 \|\rho^{T_2}\|_1, \tag{1}$$

where the notation $\|\rho^{T_2}\|_1 = Tr\left(\sqrt{\rho^{T_2}(\rho^{T_2})^\dagger}\right)$ is the trace norm of the partial transpose ρ^{T_2} [17, 23]. We resort to the following expression to compute the logarithmic negativity

$$\mathcal{LN}(\rho) = \log_2\left(\sum_j |\kappa_j|\right), \tag{2}$$

where κ_j are the negative eigenvalues of ρ^{T_2}. $\mathcal{LN}$ varies from 0 to 1; it cancels out ($\mathcal{LN}(\rho) = 0$) for unentangled states and it is maximal ($\mathcal{LN}(\rho) = 1$) for bipartite states with maximal entanglement.

2.2 QMA-EUR

Uncertainty relations limit the potential information one can gather about a system's physical properties. For two arbitrary observables $\mathcal{O}$ and $\mathcal{W}$, this uncertainty can be expressed using the standard deviation $\Delta\mathcal{O} = \sqrt{\langle\mathcal{O}^2\rangle - \langle\mathcal{O}\rangle^2}$ as [32]

$$\Delta\mathcal{O}\Delta\mathcal{W} \geq \frac{1}{2}|\langle[\mathcal{O}, \mathcal{W}]\rangle|. \tag{3}$$

However, in the framework of information theory, uncertainty relations are written in terms of the entropy. Among these entropic uncertainty relations, we find the following relation [36, 37] based on the Shannon entropy $H(\mathcal{O})$:

$$H(\mathcal{O}) + H(\mathcal{W}) \geq log_2\frac{1}{c}, \tag{4}$$

the term $\frac{1}{c}$ quantifies the complementarity of the two observables, with $c = \max_{kl}|\langle o_k \mid w_l\rangle|^2$. $|o_k\rangle$ and $|w_l\rangle$ are, respectively, the eigenvectors of $\mathcal{O}$ and $\mathcal{W}$.

Uncertainty relations can be thought of by considering two parties; Alice and Bob who agree on two measurements $\mathcal{O}$ and $\mathcal{W}$. Bob creates a particle in a desired quantum state and transmits it to Alice, who then performs one of the two measurements and informs Bob of her decision. Bob has to reduce his uncertainty regarding the outcome of Alice's measurement. Berta et al. [37] proved that in order to achieve his task and minimize the uncertainty, Bob should entangle the particle he sends to Alice to a quantum memory. This new improved uncertainty relation, named QMA-EUR is written in terms of the von Neumann entropy [37]

$$S(\mathcal{O}|B) + S(\mathcal{W}|B) \geq S(A|B) + \log_2\frac{1}{c}, \tag{5}$$

where the conditional von Neumann entropy $S(\mathcal{O}(\mathcal{W})|B) = S(\rho_{\mathcal{O}(\mathcal{W})B}) - S(\rho_B)$ quantifies the uncertainty about the result of the measurement $\mathcal{O}(\mathcal{W})$ given the information stored in the quantum memory B. $\rho_{\mathcal{O}} = \sum_k(|o_k\rangle\langle o_k| \otimes I)\rho_{AB}(|o_k\rangle\langle o_k| \otimes I)$ and $\rho_{\mathcal{W}} = \sum_l(|w_l\rangle\langle w_l| \otimes I)\rho_{AB}(|w_l\rangle\langle w_l| \otimes I)$ are the post-measurements states and ρ_B is the reduced density matrix describing the quantum memory B. Moreover, the supplementary term $S(A|B)$ in the bound of the inequality (5) quantifies the amount of entanglement between the particles A and B. In this manuscript, we choose our two measurements to be the Pauli matrices σ_x and σ_z. Therefore, we find that $c = \frac{1}{2}$. The left-hand side of the inequality is the measured QMA-EUR, and it is given by

$$U_L = -2S(\rho_B) + S(\rho_{\sigma_x B}) + S(\rho_{\sigma_z B}). \tag{6}$$

The right-hand side of the inequality is the bound constricting the estimation accuracy by Bob. It is computed using the following expression

$$U_R = \log_2\frac{1}{c} + S(\rho_{AB}) - S(\rho_B). \tag{7}$$

3 Setup

In this research, we investigate a system consisting of two spins described by a Heisenberg model. The system is subjected to the Dzyaloshinsky–Moriya interaction with a uniform external magnetic field B. The spins are assumed to be coupled through the Herring–Flicker interaction. The system's Hamiltonian can be expressed as follows

$$H = J(R)\left(\sigma_1^x\sigma_2^x + \sigma_1^y\sigma_2^y + \delta\sigma_1^z\sigma_2^z\right) + \vec{D}.(\vec{\boldsymbol{\sigma}}_1 \wedge \vec{\boldsymbol{\sigma}}_2) + B\left(\sigma_1^z + \sigma_2^z\right), \tag{8}$$

here, $\sigma_{i=1,2}^\alpha$ (with $\alpha = x, y, z$) represent the Pauli matrices. The parameter δ signifies the anisotropy factor, and $\vec{D}$ denotes the Dzyaloshinsky–Moriya interaction vector, assumed to be oriented along the z-axis, that is: $\mathbf{D}.(\boldsymbol{\sigma}_1 \wedge \boldsymbol{\sigma}_2) = \vec{D}_z(\vec{\sigma}_1^x\vec{\sigma}_2^y - \sigma_1^y\sigma_2^x)$. Furthermore, B represents the external magnetic field along the z-axis. The

Herring–Flicker coupling $J(R)$ that characterizes the interaction between the qubits is given by:

$$J(R) = \alpha_{HF} \, e^{-2R} R^{5/2} + O(R^2 e^{-2R}), \tag{9}$$

with the leading-order coefficient $\alpha_{HF} = 1.642$. The strength of the exchange interaction $J(R)$, diminishes exponentially, and it is generally considered a short-range interaction. The accompanying figure provides a visual depiction of the coupling between two spins as a function of the relative distance R (Fig. 1);

In the standard computational basis $\{\{|jk\rangle; j, k = 0, 1\}$, the Hamiltonian given by Eq. (8) can be expressed as

$$H = \begin{pmatrix} J(R)\delta + 2B & 0 & 0 & 0 \\ 0 & -J(R)\delta & 2J(R) + 2iD_z & 0 \\ 0 & 2J(R) - 2iD_z & -J(R)\delta & 0 \\ 0 & 0 & 0 & J(R)\delta - 2B \end{pmatrix}. \tag{10}$$

By performing a direct computation, we can ascertain the eigenvalues and associated eigenvectors of the Hamiltonian provided in Eq. (10)

$$E_1 = J(R)\delta + 2B, \quad |\varphi_1\rangle = |00\rangle, \tag{11}$$

$$E_2 = -J(R)\delta - 2\xi, \quad |\varphi_2\rangle = \frac{1}{\sqrt{2}}\left[\frac{J(R) + iD_z}{\xi}|01\rangle + |10\rangle\right], \tag{12}$$

$$E_3 = -J(R)\delta + 2\xi, \quad |\varphi_3\rangle = \frac{1}{\sqrt{2}}\left[\frac{-J(R) - iD_z}{\xi}|01\rangle + |10\rangle\right], \tag{13}$$

$$E_4 = J(R)\delta - 2B, \quad |\varphi_4\rangle = |11\rangle, \tag{14}$$

where $\xi = \sqrt{D_z^2 + J^2(R)}$.

The following Gibbs density operator describes the system with the Herring–Flicker interaction. This system and a reservoir are in thermal equilibrium at a temperature T

$$\rho(T) = \frac{e^{-\beta H}}{\mathcal{Z}}, \tag{15}$$

here, we define β as $\frac{1}{k_B T}$, where k_B represents the Boltzmann constant, which we conveniently set to unity. The partition function, $\mathcal{Z}$, is expressed as $\mathcal{Z} = \text{Tr}(e^{-\beta H}) = \sum_{i=1}^{4} e^{-\beta E_i}$. The resulting thermal density matrix is expressed in the calculation base as follows

$$\rho(T) = \begin{pmatrix} \rho_{11} & 0 & 0 & 0 \\ 0 & \rho_{22} & \rho_{23} & 0 \\ 0 & \rho_{32} & \rho_{33} & 0 \\ 0 & 0 & 0 & \rho_{44} \end{pmatrix}. \tag{16}$$

The elements of the density matrix are expressed as

$$\rho_{11} = \frac{e^{-\frac{J(R)\delta + 2B}{T}}}{\mathcal{Z}},$$

$$\rho_{22} = \rho_{33} = \frac{e^{\frac{J(R)\delta}{T}} \cosh(\frac{2\xi}{T})}{\mathcal{Z}},$$

$$\rho_{44} = \frac{e^{\frac{-J(R)\delta + 2B}{T}}}{\mathcal{Z}}, \tag{17}$$

$$\rho_{23} = -\frac{e^{\frac{J(R)\delta}{T}} \frac{J(R) + iD_z}{\xi} \sinh(\frac{2\xi}{T})}{\mathcal{Z}},$$

$$\rho_{32} = \rho_{23}^*,$$

with the partition function $\mathcal{Z} = 2e^{-\frac{J(R)\delta}{T}} \left(\cosh(\frac{2B}{T}) + e^{\frac{2J(R)\delta}{T}} \cosh(\frac{2\xi}{T}) \right)$.

4 Discussion and results

Here, we highlight the results of our research, wherein we analyze the behavior of quantum entanglement measured via $\mathcal{LN}(\rho)$ and QMA-EUR within a two-qubit Heisenberg model featuring Herring–Flicker coupling under the impact of Dzyaloshinsky–Moriya interaction. We perform an in-depth examination of how various critical parameters, including

Fig. 1 Variation of $J(R)$ versus the coupling distance R
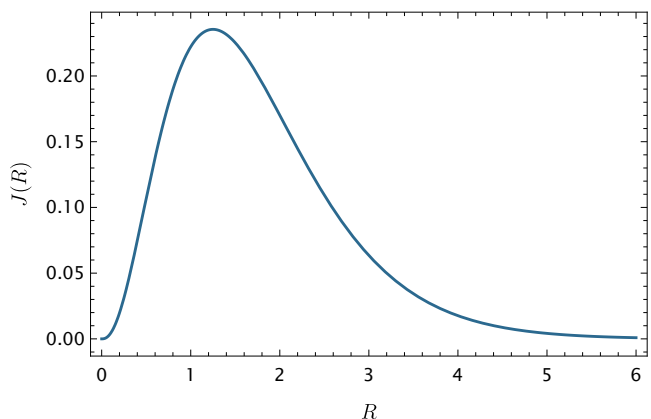
the inter-spins relative distance (R), the external magnetic field (B), the equilibrium temperature (T), the strength of DM interaction (D_z), and the anisotropy parameter (δ), impact the quantum metrics utilized in our study.

To initiate this exploration, Fig. 2 examines the impact of varying the coupling distance (R) on the QMA-EUR and thermal entanglement within the system under investigation. It is worth noting that all other system parameters are held constant, with values set to $\delta = D_z = B = 0.5$.

From Fig. 2a, d, it is worth remarking that the coupling distance R, and consequently the HF-coupling $J(R)$ influence the behavior of thermal entanglement. In this light, we notice that two intervals of R values are distinguished; for $0 < R < 1.25$, an improvement of $\mathcal{LN}(\rho)$ is observed. $R = 1.25$, which corresponds to the maximum of Herring–Flicker coupling $J(R) \approx 0.2354$, is the ideal configuration of this parameter, allowing for a maximal strengthening of entanglement. Beyond this optimal coupling distance ($R = 1.25$), $\mathcal{LN}(\rho)$ decreases and freezes into a constant value. It is clear from Fig. 2a, d that the effect of the temperature T is the most prevailing, such that entanglement decreases steadily and vanishes for growing T degrees. In Fig. 2d we recognize the phenomenon of entanglement sudden death (ESD) happening at specific critical temperatures T_c. The values of T_c where the quantum phase transition

entanglement-separability occurs, is improved for growing R in the range of $0 < R \leq 1.25$. Thereby, we find that $T_c(R = 0.5) \approx 1.244$, while $T_c(R = 1.25) \approx 1.435$. In order to explain the entanglement sudden death behavior, we thoroughly investigate the expression of $\mathcal{LN}$ used to quantify entanglement. The density matrix $\rho(T)$ (Eq. (16)) is an X state, so is its partial transpose $\rho^{T_B}(T)$. Further, we find that the eigenvalues of this latter are $\kappa_1 = \kappa_2 = \rho_{22}$, which is a positive real. The other two eigenvalues are $\kappa_{3,4} = \dfrac{(\rho_{11} + \rho_{44}) \mp \sqrt{(\rho_{11} - \rho_{44})^2 + 4|\rho_{23}|^2}}{2}$, we can clearly see that κ_4 is always positive, which leaves us with κ_3. In this specific chosen configuration of $\delta = D_z = B = 0.5$, we find that κ_3 is negative for low T degrees, but as T grows, κ_3 increases until reaching $\kappa_3 = 0$ for a specific T, which depends on the relative distance R between the two spins. This specific temperature is the ESD temperature T_c. The findings shown in Fig. 2a imply that higher strengths of the Herring–Flicker coupling between the two qubits can enhance thermal entanglement in the system under consideration at lower temperatures. This means that by regulating the system parameters and the Herring–Flicker coupling, we can somewhat shield our system against the negative impact of temperature on its quantum features, namely the amount of thermal entanglement captured here by $\mathcal{LN}(\rho)$. Moving
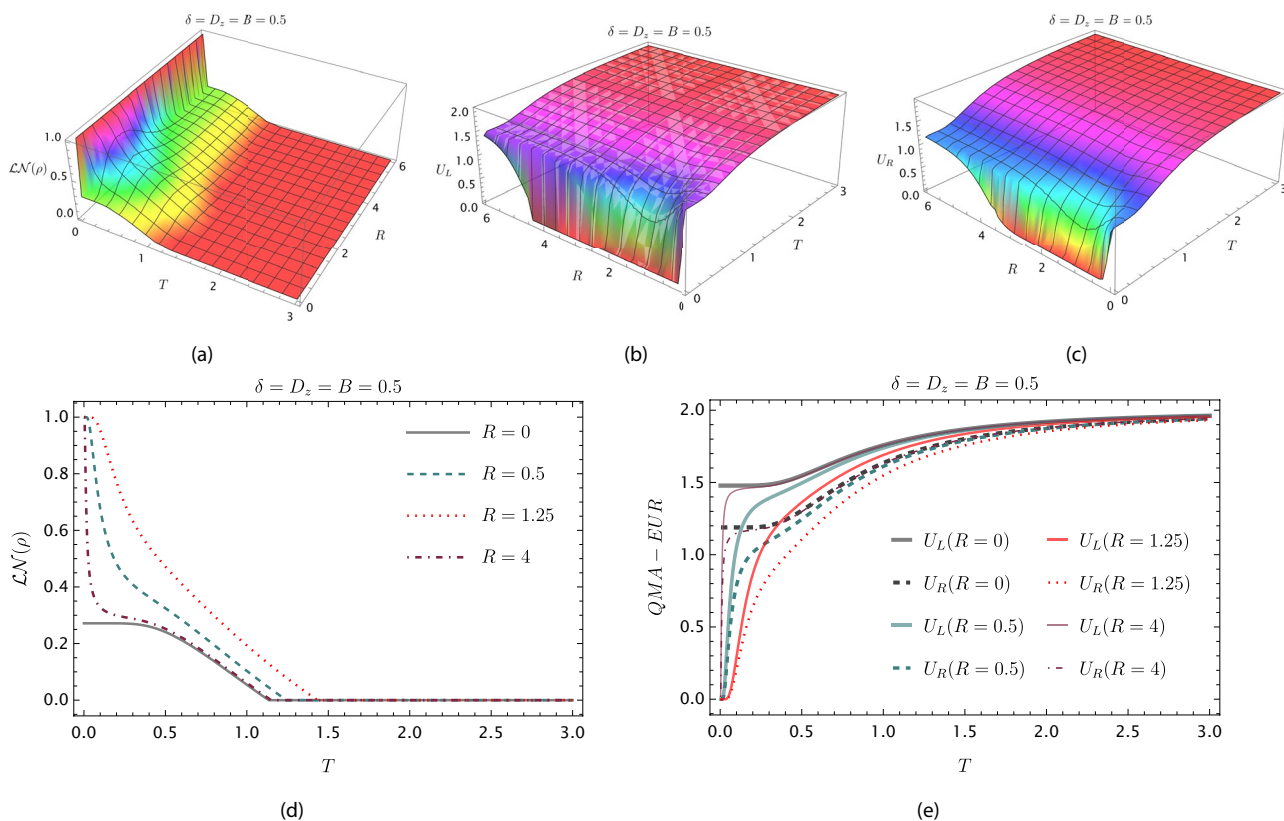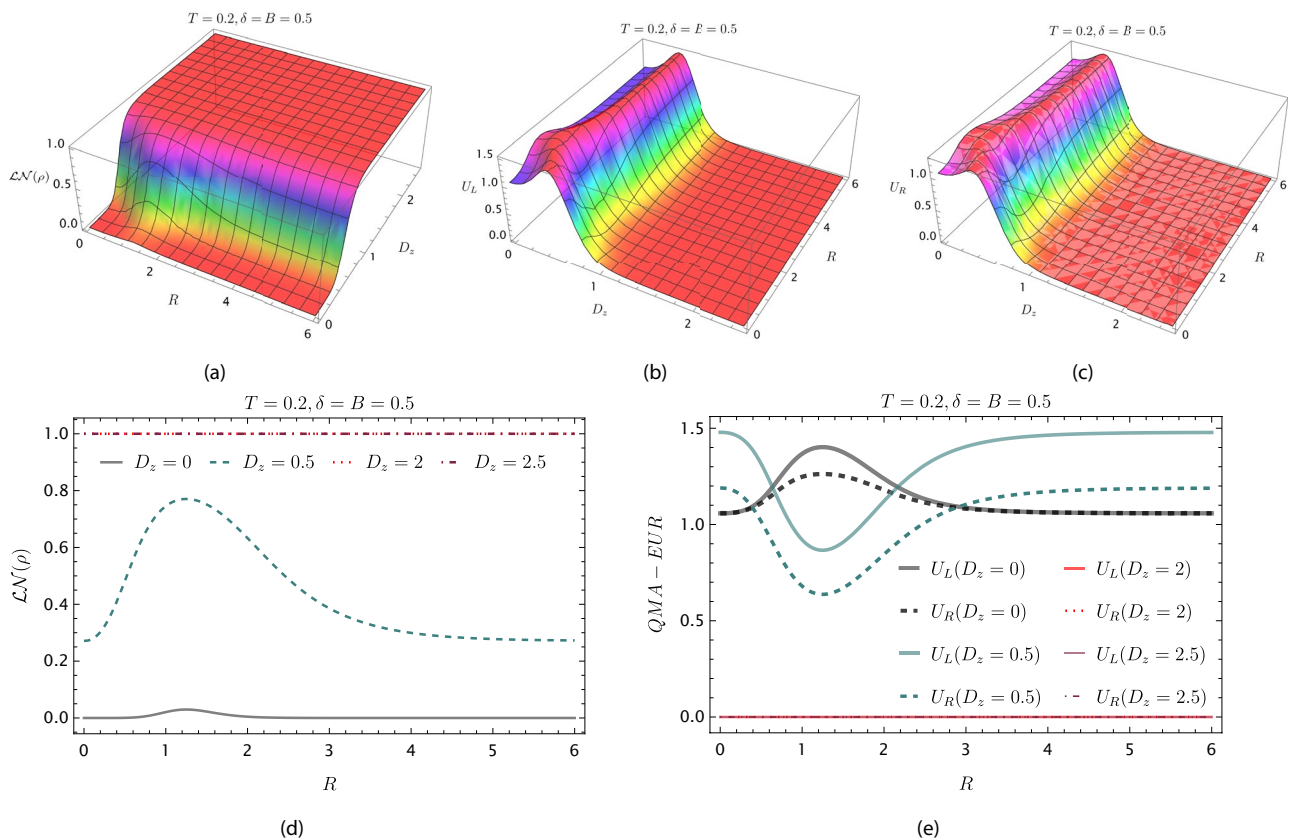

Fig. 2 $\mathcal{LN}(\rho)$ (**a–d**) and QMA-EUR (**b–c–e**) in terms of T and R when $\delta = D_z = B = 0.5$

on to Fig. 2b, c, e, where we observe that QMA-EUR displays the opposite behavior to that of thermal entanglement for different values of the coupling distance R. At lower temperatures, we observe that QMA-EUR reveals significant values for $R = 0$; i.e. in the absence of Herring–Flicker coupling. Whereas, as $T = 0$, the QMA-EUR is zero for all non-zero values of the coupling distance R. This finding indicates that introducing Herring–Flicker coupling can reduce QMA-EUR in the system at lower temperatures. As the temperature increases, QMA-EUR increases monotonically and reaches its maximal value ($U_L = U_R \rightarrow 2$) at higher temperatures. Consequently, by adequately adjusting the coupling distance R yielding higher Herring–Flicker coupling strength and by carefully selecting the other system parameters, it is possible to attenuate the harmful effects of temperature, reduce the QMA-EUR, and stabilize the amount of thermal entanglement within the investigated system.

Next, we present in Fig. 3, the impact of the DM interaction and the Herring–Flicker coupling distance on thermal entanglement and QMA-EUR in the two-qubit spin system. We fixed the remaining parameters at $T = 0.2$ and $\delta = B = 0.5$.

In Fig. 3a, d, a clear pattern emerges: when the DM interaction within the system is absent ($D_z = 0$), $\mathcal{LN}(\rho)$ becomes nonexistent. A minor, insignificant level of thermal entanglement appears at a coupling distance of $R = 1.25$, which corresponds to the peak strength of the Herring–Flicker coupling, approximately $J(R) \approx 0.2354$. Conversely, when the DM interaction becomes sufficiently strong ($D_z \geq 2$), the two spins become maximally entangled regardless of the coupling distance R between them. For small non-zero values of D_z, it is observed that $\mathcal{LN}(\rho)$ initially increases, reaching its maximum at $R = 1.25$, and then decreases to stabilize at its initial value recorded for $R = 0$. These findings underscore the ability to optimize thermal entanglement within the system by fine-tuning both the Herring–Flicker coupling and the DM interaction. In Fig. 3b, c, and e, a notable contrast emerges in the behavior of QMA-EUR compared to thermal entanglement. Regardless of the coupling distance R, it becomes apparent that QMA-EUR diminishes as D_z increases and ultimately becomes negligible for higher levels of DM interaction strength. In fact, with high values of D_z, there is a complete lack of uncertainty in the results of both measurements, σ_x and σ_z, as reflected in the conditional entropies within the QMA-EUR: $S(\rho_{\sigma_x B}) - S(\rho_B) = S(\rho_{\sigma_z B}) - S(\rho_B) = 0$. Furthermore, in the lower bound U_R, the term quantifying entanglement between the two qubits yields $S(A|B) = -\log_2(d = 2) = -1$, with d

(a)

(b)

(c)

(d)

(e)

Fig. 3 $\mathcal{LN}(\rho)$ (**a–d**) and QMA-EUR (**b, c–e**) in terms of R and D_z when $T = 0.2$ and $\delta = B = 0.5$

representing the dimension of the qubit A sent to Alice. Consequently, this indicates that the lower bound is also reduced to zero. These findings provide valuable insights into the interplay between thermal entanglement and the system's parameters. Specifically, they shed light on the fact that thermal entanglement between the two qubits exhibits a notable enhancement within a defined range of distance values. This enhancement is closely related to the augmentation in the HF coupling $J(R)$ and the presence of a substantial DM interaction. Furthermore, these observations emphasize an intriguing inverse relationship. As thermal entanglement becomes more pronounced and robust, the measure of QMA-EUR experiences a decline. This phenomenon implies a fine-tuned relationship between the level of quantum entanglement and the precision of measurements within the system. A rise in one factor corresponds to a decrease in the other. This connection can be explained theoretically by delving into quantum entanglement's nature as a type of quantum correlation. Essentially, stronger quantum correlations result in a decrease in measurement uncertainty. In simpler terms, higher entanglement leads to less uncertainty, while lower uncertainty is associated with increased entanglement.

In Fig. 4, we illustrate the variations of thermal entanglement, U_L, and U_R in the system under consideration as a function of Herring–Flicker coupling distance (R) for

different given values of (B). The other defining parameters are set to $T = 0.2$ and $\delta = D_z = 0.5$.

Figure 4a–e offer a comprehensive view of how the interplay between the coupling distance R and the external magnetic field B affects the system. Figure 4a clearly illustrates that a strong magnetic field B causes quantum entanglement to vanish, regardless of the specific value of the coupling distance R. Meanwhile, in a scenario where the temperature remains fixed at $T = 0.2$, the quantifier $\mathcal{LN}(\rho)$ approaches its maximum value of 1 when $B = 0$, regardless of the chosen value for R. Moreover, when $B = 0.5$, we observe a noteworthy trend in $\mathcal{LN}(\rho)$ as it increases with the growing value of R until reaching its peak at $R = 1.25$. This particular coupling distance corresponds to the point where the HF coupling achieves its maximum value. Subsequently, $\mathcal{LN}(\rho)$ gradually decreases and stabilizes at its initial value, which is approximately $\mathcal{LN}(\rho) \approx 0.26$, as the coupling distance R continues to increase. This trend underscores that the coupling distance between the two qubits enhances thermal entanglement within the examined system, specifically at $R = 1.25$. In contrast, Fig. 4b, c clearly demonstrate that the absence of B leads to a reduction in both U_L and U_R within the system. As the magnetic field strength, B, increases, both U_L and U_R reach their respective peaks but eventually stabilize at a consistent value of ($U_L = U_R = 1$) at higher B
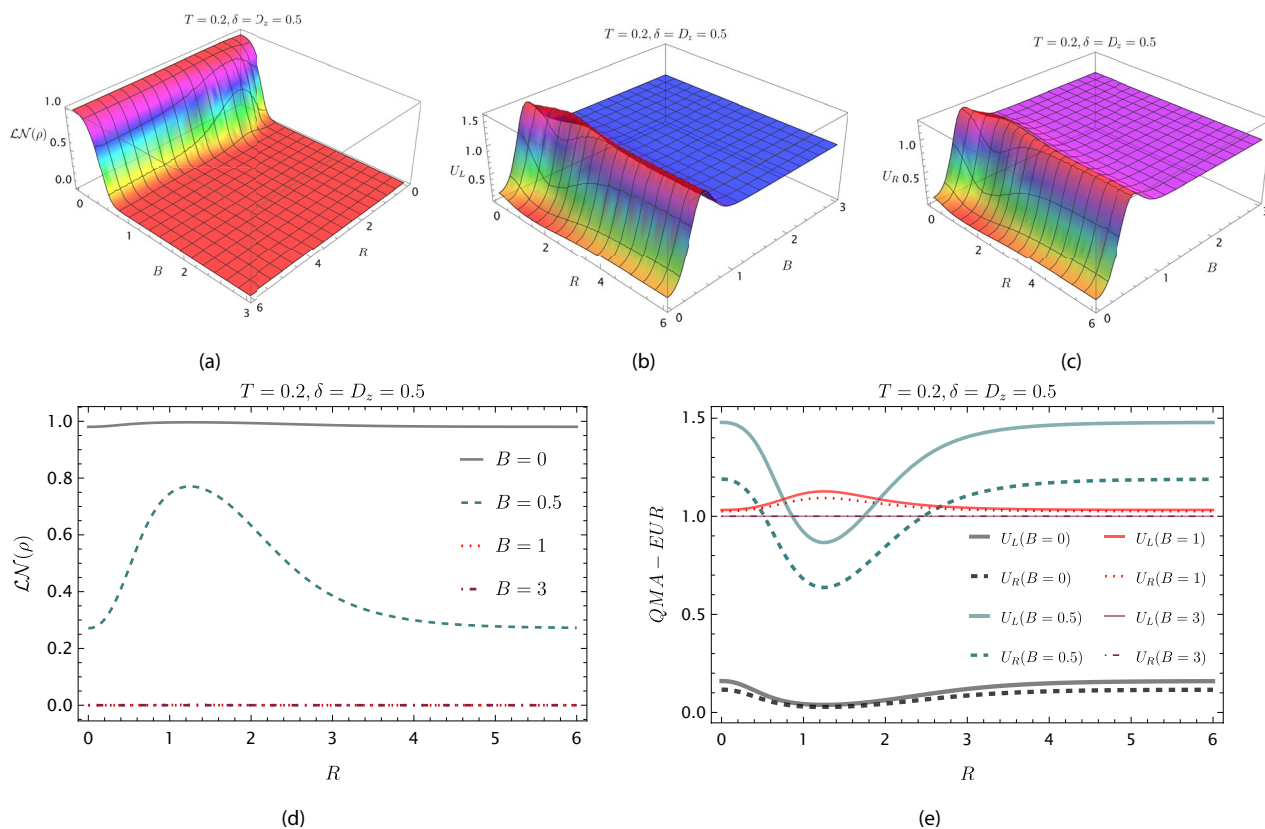

Fig. 4 $\mathcal{LN}(\rho)$ (**a–d**) and QMA-EUR (**b–c–e**) in terms of R and B when $T = 0.2$ and $\delta = D_z = 0.5$

values. In contrast, the behavior depicted in Fig. 4e reveals that QMA-EUR experiences a decrease in the absence of an external magnetic field ($B = 0$). Remarkably, it is even possible to entirely eliminate measurement uncertainty when $R = 1.25$, as we find that both U_L and U_R reach a value of zero. As the external magnetic field B is introduced into the system, QMA-EUR attains its highest value, after which, with an increase in the coupling distance R, this value gradually diminishes, reaching its minimum value at $R = 1.25$. Subsequently, it rises again to reach a stable value at higher values of the coupling distance R. Moreover, at elevated levels of the magnetic field ($B = 3$), it becomes evident that QMA-EUR remains constant, with both U_L and U_R equal to one, regardless of the specific coupling distance R.

Now, let us investigate in Fig. 5 the impact of DM interaction (D_z) on the variation of our quantum indicators when $R = 1.5$ and $\delta = B = 0.5$.

In Fig. 5a, it is evident that the strength of the DM interaction D_z plays a crucial role in mitigating the adverse effects of rising temperatures (T). When there is no DM interaction ($D_z = 0$), it is clear that $\mathcal{LN}(\rho)$ becomes null ($\mathcal{LN}(\rho) = 0$) for all temperatures, except for a slight peak occurring at nearly zero temperatures. However, with non-zero D_z values, $\mathcal{LN}(\rho)$ distinctly captures maximum thermal entanglement at lower temperatures ($T \to 0$). This entanglement gradually diminishes as temperature increases and drops to zero at critical temperatures (T_c), which are dependent on the values of D_z. Remarkably, higher DM interaction strengths allow for the maintenance of maximal entanglement even at relatively high temperatures. This is reflected in the width of the plateau regions presented in Fig. 5a. Furthermore, an increase in D_z results in raising the critical temperature at which the entangled state is lost. In Fig. 5b, it becomes clear that the amount of QMA-EUR in the system at low temperatures ($T \to 0$) is dependent on the strength of the DM interaction. For $D_z \neq 0$, both U_L and U_R reach a value of zero,

corresponding to a maximally entangled state. Conversely, in the absence of the DM interaction ($D_z = 0$), we find that $U_L = U_R = 1$. As temperature increases, QMA-EUR rises and eventually stabilizes at a value of $U_L = 2$ at higher temperatures. To summarize, the relationship between QMA-EUR and quantum entanglement within the system offers valuable insights. These two indicators display contrasting behaviors in response to the various parameters defining the Heisenberg model under investigation. By analyzing the dynamics of quantum entanglement, one can effectively anticipate the corresponding changes in QMA-EUR, and conversely, observing the fluctuations in QMA-EUR provides crucial insights into the evolving entanglement within the system. This reciprocal interaction between the two metrics sheds light on the intricate interplay of factors influencing the behavior of the studied system.

Next, we investigate in Fig. 6 the joint effect of δ (the anisotropy parameter) on the variation of thermal entanglement and QMA-EUR within the considered Heisenberg system. The other system parameters are fixed at $R = 1.25$, $B = 0.2$, and $D_z = 3$.

In Fig. 6a, it is evident that $\mathcal{LN}(\rho)$ exhibits a significant amount of thermal entanglement at lower temperatures ($T \to 0$) across all values of δ. As the temperature T increases, the thermal entanglement within the two-qubit system decreases. This decrease indicates a transition from a maximally entangled state to an entangled state, where $0 < \mathcal{LN}(\rho) < 1$. At elevated temperatures, $\mathcal{LN}(\rho)$ declines rapidly and eventually reaches zero at a critical temperature (T_c), which is contingent upon the anisotropy parameter. For instance, when $\delta = 0$, the critical temperature is approximately $T_c \approx 6.83$, while for $\delta = 2$, it is approximately $T_c \approx 7.58$. At T_c, the system assumes a separable state ($\mathcal{LN}(\rho) = 0$). Moreover, Fig. 6a highlights the role of the anisotropy parameter in enhancing thermal entanglement within the system. It is evident that the width of the plateau
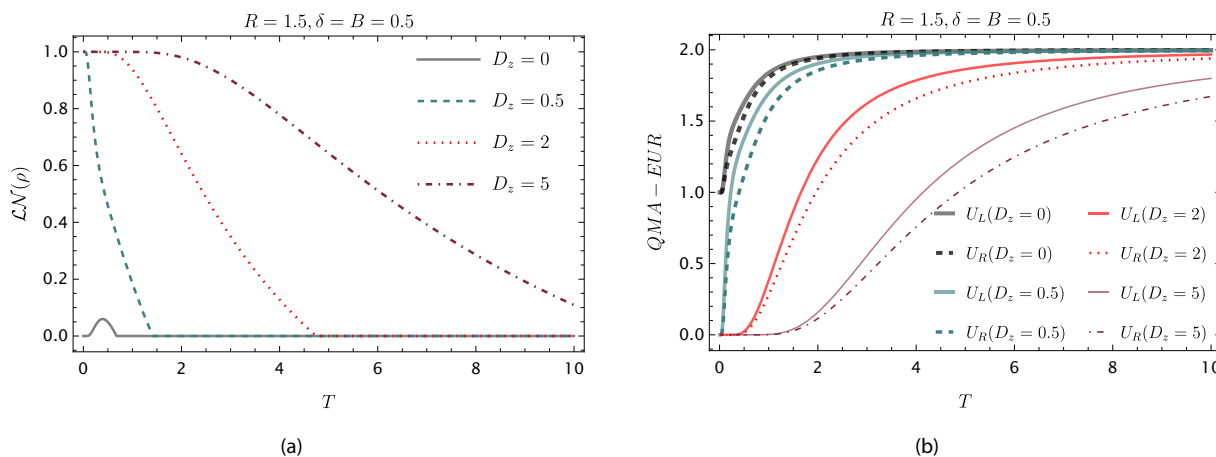

Fig. 5 $\mathcal{LN}(\rho)$ (**a**) and QMA-EUR (**b**) as a function of T for different values of D_z when $R = 1.5$ and $\delta = B = 0.5$
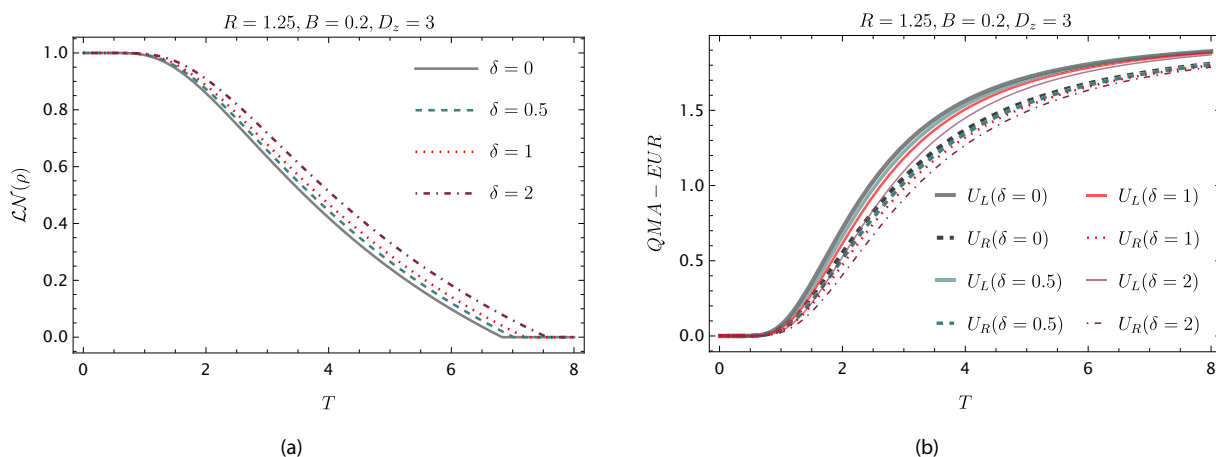
Fig. 6 $\mathcal{LN}(\rho)$ (**a**) and QMA-EUR (**b**) in terms of T for various values of δ when $R = 1.25$, $B = 0.2$ and $D_z = 3$

region in $\mathcal{LN}(\rho)$ slightly increases with higher δ. However, it is DM interaction that effectively preserves maximal entanglement with respect to temperature T (Fig. 5). In Fig. 6b, there is a clear inverse relationship between QMA-EUR and thermal entanglement. At low temperatures, QMA-EUR is consistently zero ($U_L = U_R = 0$), but as the temperature rises, QMA-EUR increases steadily to reach a maximum value for all values of δ.

Finally, we examine how the external homogeneous magnetic field (B) impacts thermal entanglement and QMA-EUR within the considered system. To do this, we plot $\mathcal{LN}(\rho)$ and QMA-EUR in terms of temperature T for various values of B, and we set the other system parameters to $R = 1.5$ and $\delta = D_z = 0.5$, as shown in Fig. 7.

Figure 7a provides valuable insights into the behavior of $\mathcal{LN}(\rho)$ in the absence of an external magnetic field (B). It is evident that $\mathcal{LN}(\rho)$ captures the maximum thermal entanglement in the ground state ($T \to 0$). As the temperature (T) increases, $\mathcal{LN}(\rho)$ declines rapidly and reaches zero at

the critical temperature ($T_c \approx 1.418$). Importantly, the T_c value at which the quantum phase transition from entanglement to separability occurs is determined by the D_z value and remains independent of the magnetic field's intensity (B). Additionally, the width of the plateau region decreases with increasing B. For $B = 1$, a small resurgence of $\mathcal{LN}(\rho)$ is noticed around $T \approx 0.2$, but it eventually vanishes at T_c. Beyond a certain threshold of B, the two-qubit Heisenberg model becomes separable even at extremely low temperatures. This implies that the presence of B with higher intensities has a negative impact on the amount of thermal entanglement, as reflected in $\mathcal{LN}(\rho)$. Analyzing Fig. 7b, we can clearly observe that QMA-EUR exhibits a consistent increase with rising temperature (T), and throughout this progression, U_L remains consistently greater than U_R. However, a noteworthy phenomenon occurs at the critical temperature (T_c), where thermal entanglement completely vanishes. At this point, QMA-EUR tends to stabilize at its maximum value, aligning perfectly with its lower bound,
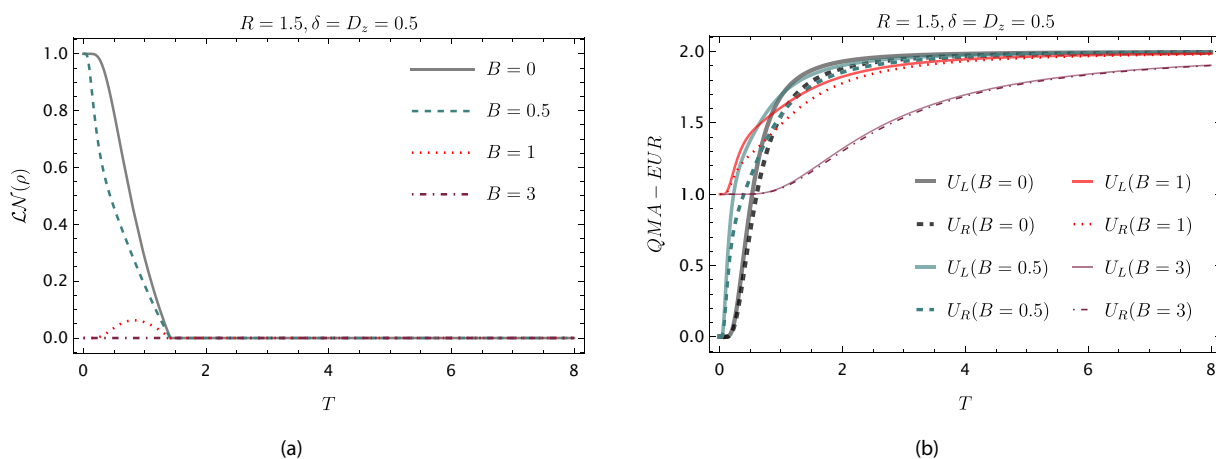

Fig. 7 $\mathcal{LN}(\rho)$ (**a**) and QMA-EUR (**b**) in terms of T for various values of B when $R = 1.5$ and $\delta = D_z = 0.5$

holding $U_L = U_R = 2$. Moreover, Fig. 7b highlights that the presence of an external magnetic field (B) enhances the QMA-EUR between the qubits in the studied system. Consequently, for low values of B ($B \to 0$), QMA-EUR commences at $U_L = U_R = 0$ when $T = 0$, and then steadily increases as temperature rises. On the other hand, for higher values of B, it initiates at a substantial value ($U_L = U_R = 1$). Overall, Fig. 7 underscores the strong connection between measurement uncertainty and the level of entanglement between the two qubits. It becomes evident that maximizing entanglement leads to the complete reduction of QMA-EUR, emphasizing the intricate interplay between these two key aspects in the system.

5 Conclusion

In summary, we have examined the relations and variations of thermal entanglement and quantum-memory-assisted entropic uncertainty (QMA-EUR) in a two-qubit one-dimensional XXZ Heisenberg spin-1/2 chain with Herring–Flicker coupling under an external homogeneous magnetic field and DM interaction at thermal equilibrium with a reservoir. Specifically, we examined the impact of Herring–Flicker coupling on thermal entanglement and QMA-EUR. It has been shown that Herring–Flicker coupling can enhance thermal entanglement against the negative impact of T and external magnetic field, specifically for the distance $R = 1.25$, which yields the maximal strength of the Herring–Flicker interaction. Our findings also demonstrate that increasing the anisotropy parameter and DM interaction strength can improve thermal entanglement in the system. Therefore, thermal entanglement between the two qubits is achieved and can be maintained by reducing the temperature and the intensities of the external magnetic field while simultaneously increasing the DM interaction and the anisotropy parameter. On the other hand, our results revealed that equilibrium temperature has a significant influence on QMA-EUR and that the latter shows marked variations according to this parameter. QMA-EUR grows for rising temperatures, reaching a steady maximum value ($U_L = U_R = 2$) at greater temperature degrees. Moreover, our analysis shows that a strong Herring–Flicker coupling can lead to a reduction in QMA-EUR, and inversely, a strong external magnetic field may lead to the expansion of QMA-EUR. It is worth mentioning that although the graphical results obtained show unequivocally that quantum entanglement and QMA-EUR have an anti-correlated relationship, demonstrating that it is possible to reduce or even eliminate measurement uncertainty by achieving and preserving maximal amounts of entanglement in quantum systems, finding an analytical expression linking directly QMA-EUR or its lower bound U_R to $\mathcal{LN}(\rho)$ for any arbitrary X-state is a difficult task. Finally, this research provides valuable insights into optimizing a two-qubit XXZ Heisenberg model with Herring–Flicker coupling to achieve quantum advantages in quantum information processing.

Declarations

References

1. M.A. Nielsen, I.L. Chuang, *Quantum Computation and Quantum Information* (Cambridge University Press, Cambridge, 2000)
2. C.H. Bennett, S.J. Wiesner, Communication via one-and two-particle operators on Einstein–Podolsky–Rosen states. Phys. Rev. Lett. **69**(20), 2881 (1992)
3. D. Deutsch, Quantum theory, the Church–Turing principle and the universal quantum computer. Proc. R. Soc. Lond. A Math. Phys. Sci. **400**(1818), 97 (1985)
4. A. Barenco, D. Deutsch, A. Ekert, R. Jozsa, Conditional quantum dynamics and logic gates. Phys. Rev. Lett. **74**(20), 4083 (1995)
5. A.K. Ekert, Quantum cryptography based on Bell's theorem. Phys. Rev. Lett. **67**(6), 661 (1991)
6. C.H. Bennett, G. Brassard, Quantum cryptography: public key distribution and coin tossing. Theor. Comput. Sci. **560**, 7 (2014)
7. C.H. Bennett, G. Brassard, C. Crépeau, R. Jozsa, A. Peres, W.K. Wootters, Teleporting an unknown quantum state via dual classical and Einstein–Podolsky–Rosen channels. Phys. Rev. Lett. **70**(13), 1895 (1993)
8. D. Bouwmeester, J.W. Pan, K. Mattle, M. Eibl, H. Weinfurter, A. Zeilinger, Experimental quantum teleportation. Nature **390**(6660), 575 (1997)
9. G.C. Fouokeng, E. Tedong, A.G. Tene, M. Tchoffo, L.C. Fai, Teleportation of single and bipartite states via a two qubits XXZ Heizenberg spin chain in a non-Markovian environment. Phys. Lett. A **384**(28), 126719 (2020)
10. G. Vallone, D.G. Marangon, M. Tomasin, P. Villoresi, Quantum randomness certified by the uncertainty principle. Phys. Rev. A **90**(5), 052327 (2014)
11. K. Mattle, H. Weinfurter, P.G. Kwiat, A. Zeilinger, Dense coding in experimental quantum communication. Phys. Rev. Lett. **76**(25), 4656 (1996)
12. S. Hill, W.K. Wootters, Entanglement of a pair of quantum bits. Phys. Rev. Lett. **78**(26), 5022 (1997)
13. W.K. Wootters, Entanglement of formation of an arbitrary state of two qubits. Phys. Rev. Lett. **80**(10), 2245 (1998)
14. W.K. Wootters, Entanglement of formation and concurrence. Quant. Inf. Comput. **1**(1), 27–44 (2001)

15. A. Uhlmann, Fidelity and concurrence of conjugated states. Phys. Rev. A **62**(3), 032307 (2000)

16. C.H. Bennett, D.P. DiVincenzo, J.A. Smolin, W.K. Wootters, Mixed-state entanglement and quantum error correction. Phys. Rev. A **54**(5), 3824 (1996)

17. A. Peres, Separability criterion for density matrices. Phys. Rev. Lett. **77**(8), 1413 (1996)

18. S. Popescu, D. Rohrlich, Thermodynamics and the measure of entanglement. Phys. Rev. A **56**(5), R3319 (1997)

19. D. Bruß, Characterizing entanglement. J. Math. Phys. **43**(9), 4237–4251 (2002)

20. G. Vidal, R.F. Werner, Computable measure of entanglement. Phys. Rev. A **65**(3), 032314 (2002)

21. M.B. Plenio, Logarithmic negativity: a full entanglement monotone that is not convex. Phys. Rev. Lett. **95**(9), 090503 (2005)

22. M. Horodecki, P. Horodecki, R. Horodecki, On the necessary and sufficient conditions for separability of mixed quantum states. Phys. Lett. A **223**, 1–8 (1996)

23. M. Horodecki, P. Horodecki, R. Horodecki, Separability of n-particle mixed states: necessary and sufficient conditions in terms of linear maps. Phys. Lett. A **283**(1–2), 1 (2001)

24. S. Lee, D.P. Chi, S.D. Oh, J. Kim, Convex-roof extended negativity as an entanglement measure for bipartite quantum systems. Phys. Rev. A **68**(6), 062304 (2003)

25. M. Mansour, Y. Oulouda, A. Sbiri, M. El Falaki, Decay of negativity of randomized multiqubit mixed states. Laser Phys. **31**(3), 035201 (2021)

26. E. Chaouki, Z. Dahbi, M. Mansour, Dynamics of quantum correlations in a quantum dot system with intrinsic decoherence effects. Int. J. Mod. Phys. B **36**(22), 2250141 (2022)

27. Z. Dahbi, M. Oumennana, K.E. Anouz, M. Mansour, A.E. Allati, Quantum Fisher information versus quantum skew information in double quantum dots with Rashba interaction. Appl. Phys. B **129**(2), 27 (2023)

28. M. Benzahra, M. Mansour, M. Oumennana, S. Elghaayda, Quantum correlations and thermal coherence in a two-superconducting charge qubit system. Laser Phys. **33**(7), 075202 (2023)

29. S. Elghaayda, A.N. Khedr, M. Tammam, M. Mansour, M. Abdel-Aty, Quantum entanglement versus skew information correlations in dipole-dipole system under KSEA and DM interactions. Quant. Inf. Process. **22**(2), 117 (2023)

30. M. Oumennana, E. Chaouki, M. Mansour, The intrinsic decoherence effects on nonclassical correlations in a dipole-dipole two-spin system with Dzyaloshinsky–Moriya interaction. Int. J. Theor. Phys. **62**(1), 10 (2022)

31. W. Heisenberg, Über den anschaulichen Inhalt der quantentheoretischen Kinematik und Mechanik. Z. Phys. **43**(3–4), 172–198 (1927)

32. H.P. Robertson, The uncertainty principle. Phys. Rev. **34**(1), 163 (1929)

33. I. Białynicki-Birula, J. Mycielski, Uncertainty relations for information entropy in wave mechanics. Commun. Math. Phys. **44**, 129–132 (1975)

34. D. Deutsch, Uncertainty in quantum measurements. Phys. Rev. Lett. **50**(9), 631 (1983)

35. K. Kraus, Complementary observables and uncertainty relations. Phys. Rev. D **35**(10), 3070 (1987)

36. H. Maassen, J.B.M. Uffink, Generalized entropic uncertainty relations. Phys. Rev. Lett. **60**(12), 1103 (1988)

37. M. Berta, M. Christandl, R. Colbeck, J.M. Renes, R. Renner, The uncertainty principle in the presence of quantum memory. Nat. Phys. **6**(9), 659–662 (2010)

38. A.K. Pati, M.M. Wilde, A.U. Devi, A.K. Rajagopal, Quantum discord and classical correlation can tighten the uncertainty principle in the presence of quantum memory. Phys. Rev. A **86**(4), 042105 (2012)

39. M.L. Hu, H. Fan, Competition between quantum correlations in the quantum-memory-assisted entropic uncertainty relation. Phys. Rev. A **87**(2), 022314 (2013)

40. M.L. Hu, H. Fan, Quantum-memory-assisted entropic uncertainty principle, teleportation and entanglement witness in structured reservoirs. Phys. Rev. A **86**(3), 032338 (2012)

41. H.M. Zou, M.F. Fang, B.Y. Yang, Y.N. Guo, W. He, S.Y. Zhang, The quantum entropic uncertainty relation and entanglement witness in the two-atom system coupling with the non-Markovian environments. Phys. Scr. **89**(11), 115101 (2014)

42. D. Mondal, A.K. Pati, Quantum speed limit for mixed states using an experimentally realizable metric. Phys. Lett. A **380**(16), 1395 (2026)

43. D.P. Pires, M. Cianciaruso, L.C. Céleri, G. Adesso, D.O. Soares-Pinto, Generalized geometric quantum speed limits. Phys. Rev. X **6**(2), 021031 (2016)

44. F. Grosshans, N.J. Cerf, Continuousvariable quantum cryptography is secure against non-Gaussian attacks. Phys. Rev. Lett. **92**(4), 047905 (2004)

45. M.J.W. Hall, H.M. Wiseman, Heisenberg-style bounds for arbitrary estimates of shift parameters including prior information. New J. Phys. **14**(3), 033040 (2012)

46. M. Oumennana, M. Mansour, Quantum coherence versus quantum-memory-assisted entropic uncertainty relation in a mixed spin-(1/2, 1) Heisenberg dimer. Opt. Quant. Electron. **55**(7), 594 (2023)

47. Y. Khedif, S. Haddadi, M.R. Pourkarimi, M. Daoud, Thermal correlations and entropic uncertainty in a two-spin system under DM and KSEA interactions. Mod. Phys. Lett. A **36**(29), 2150209 (2021)

48. A.U. Rahman, M.Y. Abd-Rabbou, S.M. Zangi, M. Javed, Entropic uncertainty and quantum correlations dynamics in a system of two qutrits exposed to local noisy channels. Phys. Scr. **97**(10), 105101 (2022)

49. A.U. Rahman, N. Zidan, S.M. Zangi, M. Javed, H. Ali, Quantum memory-assisted entropic uncertainty and entanglement dynamics: two qubits coupled with local fields and Ornstein Uhlenbeck noise. Quant. Inf. Process. **21**(10), 354 (2022)

50. D. Wang, F. Ming, A.J. Huang, W.Y. Sun, L. Ye, Entropic uncertainty for spin-1/2 XXX chains in the presence of inhomogeneous magnetic fields and its steering via weak measurement reversals. Laser Phys. Lett. **14**(9), 095204 (2017)

51. S. Haddadi, M.R. Pourkarimi, S. Haseli, Multipartite uncertainty relation with quantum memory. Sci. Rep. **11**(1), 13752 (2021)

52. L. Wu, L. Ye, D. Wang, Tighter generalized entropic uncertainty relations in multipartite systems. Phys. Rev. A **106**(6), 062219 (2022)

53. J.M. Renes, J.C. Boileau, Conjectured strong complementary information tradeoff. Phys. Rev. Lett. **103**(2), 020402 (2009)

54. F. Ming, D. Wang, X.G. Fan, W.N. Shi, L. Ye, J.L. Chen, Improved tripartite uncertainty relation with quantum memory. Phys. Rev. A **102**(1), 012206 (2020)

55. S. Liu, L.Z. Mu, H. Fan, Entropic uncertainty relations for multiple measurements. Phys. Rev. A **91**(4), 042133 (2015)

56. B.F. Xie, F. Ming, D. Wang, L. Ye, J.L. Chen, Optimized entropic uncertainty relations for multiple measurements. Phys. Rev. A **104**(6), 062204 (2021)

57. X. Zheng, G.F. Zhang, The effects of mixedness and entanglement on the properties of the entropic uncertainty in Heisenberg model with Dzyaloshinski-Moriya interaction. Quant. Inf. Process. **16**, 1 (2017)

58. A.J. Huang, J.D. Shi, D. Wang, L. Ye, Steering quantummemory-assisted entropic uncertainty under unital and nonunital noises via filtering operations. Quant. Inf. Process. **16**(2), 46 (2017)

59. A.J. Huang, D. Wang, J.M. Wang, J.D. Shi, W.Y. Sun, L. Ye, Exploring entropic uncertainty relation in the Heisenberg XX

model with inhomogeneous magnetic field. Quant. Inf. Process. **16**, 204 (2017)

60. M. Asoudeh, V. Karimipour, Thermal entanglement of spins in an inhomogeneous magnetic field. Phys. Rev. A **71**(2), 022308 (2005)

61. Q. Liang, Quantum correlations in a two-qubit Heisenberg XX model under intrinsic decoherence. Commun. Theor. Phys. **60**(4), 391 (2013)

62. G.F. Zhang, S.S. Li, Thermal entanglement in a two-qubit Heisenberg XXZ spin chain under an inhomogeneous magnetic field. Phys. Rev. A **72**(3), 034302 (2005)

63. M. Oumennana, A.U. Rahman, M. Mansour, Quantum coherence versus non-classical correlations in XXZ spin-chain under Dzyaloshinsky–Moriya (DM) and KSEA interactions. Appl. Phys. B **128**(9), 162 (2022)

64. M. Oumennana, Z. Dahbi, M. Mansour, Y. Khedif, Geometric measures of quantum correlations in a two-qubit heisenberg XXZ model under multiple interactions effects. J. Russ. Laser Res. **43**(5), 533–545 (2022)

65. Z. Dahbi, M. Oumennana, M. Mansour, Intrinsic decoherence effects on correlated coherence and quantum discord in XXZ Heisenberg model. Opt. Quant. Electron. **55**(5), 412 (2023)

66. J.L. Li, F. Ming, X.K. Song, L. Ye, D. Wang, Characterizing entanglement and measurement's uncertainty in neutrino oscillations. Eur. Phys. J. C **81**(8), 728 (2021)

67. D. Wang, F. Ming, X.K. Song, L. Ye, J.L. Chen, Entropic uncertainty relation in neutrino oscillations. Eur. Phys. J. C **80**, 1–9 (2020)

68. F. Ming, X.K. Song, J. Ling, L. Ye, D. Wang, Quantification of quantumness in neutrino oscillations. Eur. Phys. J. C **80**, 1–9 (2020)

69. J.L. Li, F. Ming, X.K. Song, L. Ye, D. Wang, Quantumness and entropic uncertainty in curved space-time. Eur. Phys. J. C **82**(8), 726 (2022)

70. K.K. Sharma, Herring-Flicker coupling and thermal quantum correlations in bipartite system. Quant. Inf. Process. **17**, 1–11 (2018)

71. A. Ait Chlih, N. Habiballah, M. Nassik, D. Khatib, Entanglement teleportation in anisotropic Heisenberg XY spin model with Herring-Flicker coupling. Mod. Phys. Lett. A **37**(06), 2250038 (2022)

72. Z. Huang, S. Kais, Entanglement as measure of electron-electron correlation in quantum chemistry calculations. Chem. Phys. Lett. **413**(1–3), 1 (2005)

73. C. Herring, M. Flicker, Asymptotic exchange coupling of two hydrogen atoms. Phys. Rev. **134**(2A), A362 (1964)